IL NUOVO CIMENTO Vol. 37 C, N. 4 Luglio-Agosto 2014
DOI 10.1393/ncc/i2014-11786-2

Communications: SIF Congress 2013

Search for a SM Higgs boson in the diphoton plus E_T^{MISS} channel

S. M. Mazza(*)
Università di Milano - Milano, Italy

ricevuto il 3 Marzo 2014; approvato il 19 Maggio 2014

Summary. — In this paper I discuss the search for a Standard Model (SM) Higgs boson in the diphoton plus missing transverse energy (missing E_T or E_T^{MISS}) channel using $20.7\,\mathrm{fb}^{-1}$ of data recorded by the ATLAS detector in the year 2012. Higgs boson at LHC can be generated through different processes: gluon-gluon fusion ($\sim 85\%$), vector boson fusion ($\sim 10\%$), W/Z associated production ($\sim 5\%$) and top-antitop fusion ($< 1\%$). The applied selection is optimized to isolate events from Higgs boson production associated with a W or Z boson requiring the presence of E_T^{MISS} from Z/W decay into neutrinos in addition to two isolated energetic photons. The sensitivity of this analysis is presented and found to be at a level above 5 times the predicted Standard Model cross-section.

PACS 14.70.Bh – Photons.
PACS 14.80.Bn – Standard-model Higgs bosons.
PACS 13.38.Be – Decays of W bosons.
PACS 13.38.Dg – Decays of Z bosons.

1. – Introduction

The Higgs boson was recently discovered by the ATLAS [1] and CMS [3] experiments at the international laboratories of CERN (Geneve). The Higgs boson is a crucial particle to explain the Electroweak simmetry breaking in the Standard Model (SM). The Higgs boson at LHC is produced in proton-proton collisions. There are four different production modes. Gluon-gluon fusion production process is the leading one and takes up to the 85% of the phase space. Vector boson fusion production takes up to 10% of the phase space. Associated production with Z and W (Higgs-strahlung) has a final state composed of a Higgs boson and a W or Z boson, it takes a small part of the phase space, roughly 5%. Top-antitop fusion is the less frequent case, $< 1\%$ of the phase space.

(*) E-mail: simone.mazza@mi.infn.it

The Large Hadron Collider (LHC) is an accelerator of protons and heavy ions located at CERN (Geneve). The tunnel where the collider is located is 27 km long and about 100 meters underground. At LHC two proton beams travel in two separated vacuum chambers, they are accelerated in RF resonant cavities and bent by super-conducting magnets. The two beams encounter in four point across the accelerator ring corresponding to the four main experiments: ALICE, ATLAS, CMS, LHCb. The center-of-mass energy was at first 7 TeV in 2010-1011, then it was raised to 8 TeV in 2012 and in the near future, after a technical shutdown of a couple of years it will be raised to 14 TeV.

ATLAS (A Toroidal LHC ApparatuS) is a general-purpose detector, it was built to take advantage of the full discovery potential of the accelerator. One of the main purposes was the discovery of the Higgs boson. However, other physics channels are under study, including the search for supersymmetric particles, a more accurate analysis of the top physics, CP violation in the decay of B mesons. The detector is cylinder-shaped with 12 meter radius and 44 meter length. From the inside there are the inner detector, the solenoidal magnet, the calorimeters (electromagnetic and hadronic) and the muon chambers (immersed in a thoroidal magnetic field).

In 2012 the beam bunches collided every 50 ns. The trigger system successfully reduces the input bunch crossing frequency of 20 MHz to an average of 400 Hz. The ATLAS trigger system is composed of three different levels, the first level is hardware and it is implemented in the detector, the other two layers are software.

2. – Photon and missing transverse energy reconstruction

2˙1. *ATLAS coordinate system.* – ATLAS uses a right-handed coordinate system with its origin at the nominal interaction point (IP) in the centre of the detector and the z-axis along the beam pipe. The x-axis points from the IP to the centre of the LHC ring, and the y-axis points upward. Cylindrical coordinates $(r; \phi)$ are used in the transverse plane, ϕ being the azimuthal angle around the beam pipe. The pseudorapidity is defined in terms of the polar θ angle as $\eta = \ln \tan(\theta/2)$. $(\eta; \phi)$ are in radians. Transverse quantities are defined as (for example) $E_T = \sqrt{E_x^2 + E_y^2}$, where $E_{x,y}$ is the energy projected in (x, y). The distance in angle is defined as $\Delta R = \sqrt{\Delta\eta^2 + \Delta\phi^2}$.

2˙2. *ATLAS detector structure.* – The detector is composed of subsequent layers of detectors, every detector has a cylinder-shaped part (barrel) alongside the beam pipe covering the $\eta \lesssim 1.4$ region and an end-cap part perpendicular to the beam pipe covering the $1.4 \lesssim \eta \lesssim 5$ region. This onion-like structure has the purpose of recognizing different objects using information from all the detectors.

The first layer is the inner detector, placed inside a 2 T magnetic field, that is composed of three sub-layers (pixel detectors, microstrip detectors and drift tubers). It is used to measure tracks of charged particles and to detect secondary vertices.

The second layer is the electromagnetic calorimeter, outside the magnetic field. The EM calorimeter is a sampling calorimeter made of alternate parts of liquid argon for active medium and lead for passive medium. Inside the liquid-argon fraction the electrodes and absorbers bent in an accordion shape are contained. Using this kind of structure the full azimutal angle ϕ is covered without non-sensitive regions. The calorimeter is segmented in both η and ϕ to measure the position of the electromagnetic particle shower. The energetic resolution is $\frac{\sigma}{E} = \frac{10\text{–}17\%}{\sqrt{E}} \oplus 0.7\%$. The calorimeter is composed of three layers with different segmentation; the first layer, 3–5 radiation length, (pre-sampler) is a thin

layer with $\eta \times \psi = (0.003\text{–}0.006) \times 0.025$ segmentation made only of liquid argon, the second layer, 4–15 radiation lengths, and the third layer, until 17 radiation lengths, have $\eta \times \psi = (0.025\text{–}0.050) \times 0.025$.

The third layer is the hadronic calorimeter, it covers a pseudo-rapidity region of $|\eta| < 4.9$. Its purpose is to absorb energy from particles that pass cross the EM calorimeter, but interact via the strong force; these particles are primarily jets of hadrons. The passive material is steel, with scintillating tiles that measure the energy deposited. The end-cap sections of the hadronic calorimeter are contained within the forward EM calorimeter's cryostat, and use liquid argon as well, while copper and tungsten plates are used as absorbers. The calorimeter is divided in cells of granularity $\Delta\eta \times \Delta\phi = 0.1 \times 0.1$. The overall thickness of the calorimeter is 11 interaction lengths in the $\eta = 0$ region.

The muon spectrometer is the most external element in the ATLAS detector, thus defining its total size. It cover the calorimeters and has the purpose to measure with high precision the muon momentum, using the magnetic field generated by the external toroid.

2˙3. *Photon reconstruction and identification.* – The photon reconstruction is seeded from clusters of energy deposits in the electromagnetic calorimeter. The reconstruction is designed to separate electrons, unconverted photons, and converted photons, which arise from conversions of photons in the detector material to electron-positron pairs. The clusters are matched to tracks and to conversion vertex candidates, which have been reconstructed in the inner detector and extrapolated to the second layer of the calorimeter [8]. Clusters without any matching track or conversion vertex are classified as unconverted photon candidates. Clusters with a matching vertex reconstructed from one or two tracks are converted photon candidates. The efficiency of the photon reconstruction is about 96.5% averaged over the transverse energy E_{T} and η spectra expected for photons from a Higgs boson decay.

The energies of the clusters are calibrated, separately for electrons, unconverted and converted photon candidates, to account for energy losses upstream of the calorimeter and for energy leakage outside of the cluster. The energy calibration for data is refined by applying η-dependent correction factors.

The identification of photons is based on shower shapes measured in the electromagnetic calorimeter. An initial loose cut-based selection, used also at trigger level, is based on shower shapes in the second layer of the electromagnetic calorimeter, as well as the energy deposition in the hadronic calorimeter. A tighter identification adds information from the finely segmented strip layer of the calorimeter, which provides good rejection of hadronic jets where a neutral meson carries most of the jet energy.

2˙4. *Isolation.* – To further suppress hadronic background, a calorimetric isolation requirement is applied. The isolation transverse energy E_T^{isol} is estimated by summing the transverse energy of positive-energy topological clusters (topological clusters are three-dimensional clusters of variable size, built by associating calorimeter cells on the basis of the signal-to-noise ratio) reconstructed in the electromagnetic and hadronic calorimeters in a cone of $\Delta R = 0.4$ around the photon candidate, where the region within 0.125×0.175 in $\eta \times \phi$ around the photon barycentre is excluded. E_T^{isol} is corrected for leakage of the photon energy outside the excluded region and for the contribution from underlying event (soft processes of partons in the same protons of the hard interacting partons). A photon is isolated if $E_T^{isol} < 6\,\mathrm{GeV}$.

2˙5. *The diphoton invariant mass.* – The mass measurement of the new particle in the diphoton channel rely mostly on the photon energy reconstruction and calibration and on the reconstruction of the angle between the photons through the expression: $M_{\gamma\gamma} = \sqrt{2E_1E_2(1-\cos(\theta))}$ with E_1 and E_2 the energies of the leading and subleading photons and θ the angle between the two photons.

2˙6. *Primary vertex definition.* – The selection of the primary vertex is relevant for three aspects of the analysis: the estimation of the invariant mass of the diphoton system, the selection of the jets associated with the hard interaction and the track isolation. The primary vertex selection method is documented in [10]. It is based on a neural network (NN) multi layer perceptron (MLP) combining various inputs (such as the sum of the P_T of the tracks, sum of P_T^2, vertex of the two main photons).

2˙7. *Missing E_T.* – The most important object for my analysis is the missing transverse energy [9], from now on called in short E_T^{MISS}. This quantity is closely related to invisible objects, such as neutrinos that have a very low interaction rate and cannot be directly revealed in the ATLAS detectors. After the reconstruction of all the other objects in the event (jets, photons, electrons...) using information from calorimeters, trackers and muon chambers, all the transverse energy deposits are summed: the sum should be near zero in the transverse plane if there are no invisible objects, the quantity counterbalancing the resulting sum is E_T^{MISS}. It is defined as

$$E_T^{MISS} = \sqrt{(E_x^{MISS})^2 + (E_y^{MISS})^2}, \tag{1}$$

where E_x^{MISS} and E_y^{MISS} are the missing energy projected onto the x- and y-axis, respectively, E_T^{MISS} is reconstructed as explained in the following section.

The reconstruction of E_T^{MISS} has several problems. Every hard event is accompanied by several soft particles and jet coming from underlying event and pileup (energy deposits from previous interactions). One of the hardest task in the missing energy recontruction is the treatment of these soft contributions. Another problem is that the detector is made to cover the largest possible acceptance in η but there is always the possibility that an energetic particle crosses the junction zone between the barrel and the end-caps or semi-collinear to the beam axis. Furthermore dead regions in the detector or external high energy particles (cosmic rays) might degrade the reconstruction. All these effects results in fake reconstructed E_T^{MISS}.

2˙8. *Reconstruction and calibration of E_T^{MISS}.* – The E_T^{MISS} reconstruction includes contribution from different parts of the detector: energy reconstructed in the calorimeters and muon spectrometer. The reconstruction of the E_T^{MISS} is made by summing of the cells of the calorimeter, each term is calculated from the negative sum of calibrated cell energies projected onto the x- and y-direction. The calorimeter cells are calibrated back propagating the calibration of the associated high P_T parent object, with the following order: electrons, photons, hadronically decaying τ and finally μ. Cells not associated to any object (electrons, photons, muons, jets...), but associated to reconstructed topological clusters, are also taken into account in the E_T^{MISS} reconstruction (without recalibration). Tracks are added to recover the low P_T particles that do not reach the calorimeter. Muons reconstructed in the inner detector are used to cover areas not covered by the muon spectrometer.

3. – Event selection

3˙1. *Data sample.* – The data sample used in this analysis corresponds to the full dataset recorded up to the LHC long shutdown started December 17, 2012. After the application of data-quality requirements, the data samples amount to $20.7 \pm 0.7\,\text{fb}^{-1}$ at $\sqrt{s} = 8\,\text{TeV}$. The data were recorded with instantaneous luminosity varying between $1\times10^{32}\,\text{cm}^{-2}\,\text{s}^{-1}$ and $7.8\times10^{33}\,\text{cm}^{-2}\,\text{s}^{-1}$. The number of interactions per bunch crossing has a mean of 20.4 for the data taken in 2012. The simulation is corrected to reflect the distribution of interactions per bunch crossing and the spread of the z position of the primary vertex observed in data. The Monte Carlo simulation of the Higgs signal production is made using the Powheg + Phytia generator [5,4], that is a next-to-leading-order generator, for the gluon-gluon fusion and vector boson fusion processes. For the other processes the Pythia generator is used, that is a leading-order generator. The Geant simulator [6] is used to simulate the detector behavior.

The data sample considered in this analysis was selected using a diphoton trigger. In the last step of the triggering chain, two clusters formed from energy depositions in the electromagnetic calorimeter are required. Transverse energy threshold, for the $\sqrt{s} = 8\,\text{TeV}$ data sample, are 35 GeV and 25 GeV on the leading (most energetic) and subleading (next-to-most energetic) clusters, respectively. In addition, loose criteria are applied on the shapes of the electromagnetic clusters to require that they match the expectations for electromagnetic showers initiated by photons.

3˙2. *Event and candidate selection.* – I require events passing the diphoton trigger selection to contain at least two reconstructed photon candidates in the fiducial region of the calorimeter, $|\eta_{S2}| < 2.37$ but excluding the crack region, $1.37 < |\eta_{S2}| < 1.56$, where η_{S2} is the pseudorapidity measured using the second layer of the electromagnetic calorimeter. To ensure well-reconstructed photon candidates, I apply further quality requirements to the reconstructed clusters (concerning the status of the detector and the calorimeter cells). Similarly, I reject converted-photon candidates reconstructed from tracks going through dead modules of the innermost pixel layer, strongly decreasing the misidentification of electrons as converted photons. I apply further criteria to the two highest-E_T photon candidates. I require the leading photon candidate to have $E_\text{T} > 40\,\text{GeV}$, and the subleading photon candidate to have $E_\text{T} > 30\,\text{GeV}$. I apply tighter identification criteria to both photon candidates. Furthermore, I require both photon candidates to be isolated.

With this selection, I observed 118 893 diphoton candidates in the mass range between 100 and 160 GeV in the $\sqrt{s} = 8\,\text{TeV}$ data sample.

3˙3. E_T^{MISS} *selection.* – I require the events passing the initial selection to have a value of $E_T^{MISS} > 80\,\text{GeV}$. I reconstruct the E_T^{MISS} recalibrating the contributions of all the objects (electrons, photons, muons, jets...). In fig. 1 we can see the effect of the selection on the $M_{\gamma\gamma}$ spectrum and the number of selected events after different cuts in E_T^{MISS}.

The idea of the analysis is selecting the associated production mode over the gluon-gluon, vector boson fusion and top-antitop production. For this reason I calculated, using Monte Carlo signal samples, the number of events for every production mode in the model after different selections. We can see in fig. 2 the percentual composition of the Higgs production modes after different E_T^{MISS} selections; after the $E_T^{MISS} > 80\,\text{GeV}$ selection the associated production mode (WH, ZH) is $\sim 50\%$ of the phase space (instead of the initial $\sim 5\%$).

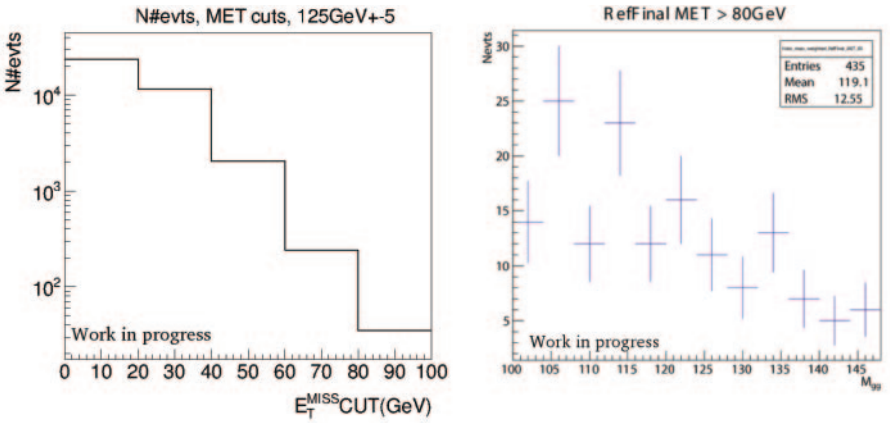

Fig. 1. – Data for full 2012 ATLAS data taking, with a total integrated luminosity of $\mathcal{L} = 20.7\,\mathrm{fb}^{-1}$, passing diphoton selection and E_T^{MISS} cuts. Left plot: Number of events remaining in the interval $[120, 130]$ GeV after different selection in E_T^{MISS}. Right Plot: $M_{\gamma\gamma}$ invariant-mass shape after the $E_T^{MISS} > 80\,\mathrm{GeV}$ cut.

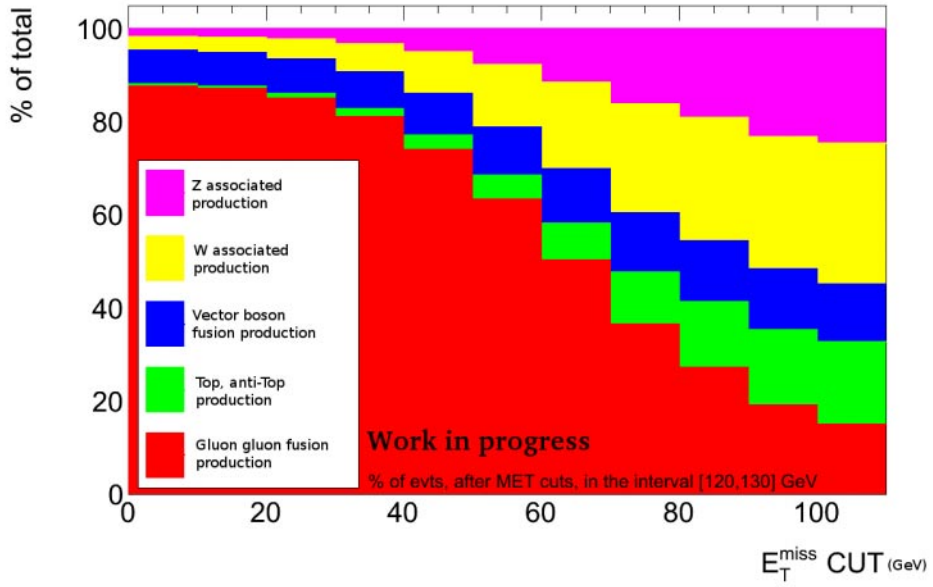

Fig. 2. – Fraction of expected signal events from different production modes in the interval $[120, 130]$ of $M_{\gamma\gamma}$ after E_T^{MISS} cuts normalized using the cross section of the processes. Plot made using Monte Carlo Higgs boson samples with $M_H = 125\,\mathrm{GeV}$. With high E_T^{MISS} cuts the associated production and top-antitop production reach a higher fraction of total signal events than gluon-gluon and vector boson fusion production.

4. – Signal and background model

4·1. *Signal model.* – The first ingredient I need for this kind of analysis is an analytic model of the shape of the Higgs signal in the reconstructed diphoton invariant-mass distribution. The model is then fitted simultaneously on a series of Monte Carlo signal samples built with different Higgs boson masses, from 100 GeV to 150 GeV with 5 GeV step. The adopted model [1] I used is a weighted sum of two different PDFs: the sum of a Gaussian and a Crystal Ball function (eq. (2)). The Crystal Ball function [7] (CB) is a probability density function commonly used to model various lossy processes in high-energy physics. It consists of a Gaussian core portion and a power-law low-end tail, below a certain threshold. The function itself and its first derivative are both continuous. The sum with a Gaussian has the purpose of describing the high and long tails of the PDFs for the Higgs signal. Some parameters of the model depend linearly on the Higgs boson mass and some parameters are fitted but with the same value for all Higgs boson masses (eq. (3)). The parameter $0 \leq f_{CB} \leq 1$ is the fraction of CB and Gaussian.

$$F(M_{\gamma\gamma}) = f_{CB} \cdot CB(M_{\gamma\gamma}) + (1 - f_{CB}) \cdot Gaus(M_{\gamma\gamma}). \tag{2}$$

I fitted simultaneously for every mass after the E_T^{MISS} selection of $E_T^{MISS} > 80\,\text{GeV}$. In table I are the fit results. The parameters are defined in eq. (3).

$$\begin{aligned}
k_{GA} &= \text{fixed for all masses but fitted,}\\
f_{CB} &= \text{fixed for all masses but fitted,}\\
n_{CB} &= 10,\\
\mu_{CB} &= M_H + \mu_{CB}(125\,\text{GeV}) + \Delta_{\mu_{CB}} \cdot (M_H - 125),\\
\sigma_{CB} &= \sigma_{CB}(125\,\text{GeV}) + \Delta_{\sigma_{CB}} \cdot (M_H - 125),\\
\alpha_{CB} &= \alpha_{CB}(125\,\text{GeV}) + \Delta_{\alpha_{CB}} \cdot (M_H - 125),\\
\mu_{GA} &= \mu_{CB},\\
\sigma_{GA} &= k_{GA} \cdot \sigma_{CB},
\end{aligned} \tag{3}$$

where μ_{CB} and Δ_μ are the linear parametrization for the center of the CB, σ_{CB} and Δ_σ are the linear parametrization for the σ of the CB, α_{CB} and Δ_α are the linear parametrization for the α parameter of the CB. The k_{GA} parameter is equal to $\frac{\sigma_{CB}}{\sigma_{GA}}$. The center of the Gaussian is equal to the center of the CB. f_{CB} is the parameter from eq. (2).

The number of events for every Higgs boson mass is calculated from the Monte Carlo samples and is fitted as well with a 3rd-order polynomial, for Higgs mass of 125 GeV the number of expected event with $E_T^{MISS} > 80\,\text{GeV}$ selection is ~ 2.3 events for $L_{int} = 20.7 \pm 0.7\,\text{fb}^{-1}$.

4·2. *Background fit.* – The second ingredient I need for the analysis is a model describing all the background processes in the diphoton invariant reconstructed mass. To decide what is the best analytic function to describe the data I created a realistic background shape using a combination of different Monte Carlo background samples. The Monte Carlo samples I used are for the processes: gamma jet sample, diphoton sample, $Z \to l^+l^- + \gamma\gamma$, $W + \gamma$, $W \to l\nu + \gamma\gamma$, $t\bar{t} + \gamma\gamma$, $t\bar{t} + \gamma$. I tried to fit the resulting sample with different analytic functions. Then I chose the best fitting function looking at the

TABLE I. – *Fit results for the sum of all the Higgs production processes of the signal model on Monte Carlo samples of Higgs signal (with different theorized masses) after the selection* $E_T^{MISS} > 80\,\text{GeV}$ (n_{CB} *fixed to* 10).

μ_{CB} (125 GeV) (MeV)	Δ_μ (MeV/GeV)	σ_{CB} (125 GeV) (GeV)	Δ_σ (MeV/GeV)
-349.123 ± 0.004	-2.8 ± 0.2	1.76 ± 0.05	11.7 ± 0.3
α_{CB} (125 GeV)	Δ_α (%/GeV)	f_{CB} (%)	k_{GA}
1.54 ± 0.02	0.0036 ± 0.0004	99.2 ± 0.3	14 ± 0.3

fit χ^2 and the spurious signal (the probability that an analytic function generate contribution to the signal peak). Afterwards I extracted the values of the parameters of the chosen analytic function from a fit on real data (outside the invariant mass region where the Higgs boson peak is situated), having thus a completely data-driven background function.

In my analysis the number of events after the selection is low, for this reason the selected sample is prone to statistical fluctuations. Fitting with a polynomial could result in describing the fluctuations and generate spurious signal that would change the output of the statistical analysis. An exponential function like $e^{A+Bx+Cx^2}$ is smoother and describes better the background sample after the $E_T^{MISS} > 80\,\text{GeV}$ cut. Because of these considerations I decided to use the exponential of a second-order polynomial to parameterize the background after the E_T^{MISS} selection.

5. – Systematic errors

The systematics errors taken into account from literature [2] are: systematic uncertainty on the diphoton mass resolution (width of the resonant peak), theoretical and experimental uncertainties on the number of expected signal events. I evaluated the systematic error of the E_T^{MISS} selection on the number of expected signal events.

5˙1. *Systematic errors from* E_T^{MISS} *selection.* – I evaluated the systematic errors under the assumption of no correlation between photons, jets and soft terms. I used Monte Carlo samples of Higgs boson with mass 125 GeV for each production process. To evaluate the systematic error I reconstructed the E_T^{MISS} value after shifting (up and down) the nominal energy values of each object (photons, electrons, jets, soft terms) by the associated error on the energy. Then I evaluated the change on the number of signal events after applying selection on the modified value of E_T^{MISS}. I found that in general, Jets are the main source of uncertainty, furthermore for the production processes of gluon-gluon fusion and vector boson fusion the greatest uncertanty is given by soft terms. I evaluated the final systematic errors with a quadratic sum of all the error sources mediated on all production modes with a weighted sum using the expected number of signal events. The resulting total systematics on the number of expected signal events for the $E_T^{MISS} > 80\,\text{GeV}$ selection are +9% up and −4.8% down. The overview of all the systematic errors I used is in table II.

TABLE II. – *Systematic errors on the invariant mass resolution (first row) and on the expected number of signal events.*

Systematic source	% value
Diphoton invariant mass resolution uncertainty	20%
Uncertainties on the number of signal events	
Theoretical uncertainty	10%
Luminosity uncertainty	3.6%
Trigger uncertainty	0.5%
Isolation uncertainty	0.5%
Mass energy scale	0.3%
Identification efficiency uncertainty	10.8%
E_T^{MISS} uncertainty up	9%
E_T^{MISS} uncertainty down	4.8%

6. – Statistical analysis and results

In this section I will report the result of the statistical analysis on the full 2012 data taking of ATLAS corresponding to $\mathcal{L} = 20.7\,\text{fb}^{-1}$ passing the diphoton plus $E_T^{MISS} > 80\,\text{GeV}$ selection. I used the approach and formulae from ref. [11] using asymptotic methods based on results due to Wilks [12] and Wald [13]. Asymptotic formulae are proven to work even with the low number of events after the selection, this result was verified with toy Monte Carlo in [11].

The signal model and background model used are the ones discussed before. The parameters of the background function are fitted on the sidebands $[100, 120]$ GeV and $[130, 150]$ GeV of the diphoton invariant-mass distribution of data. The signal model is built with the parameters from table I. The nuisance parameters for the expected number of signal events and mass resolution used are the ones from table II.

The expected number of signal events for the selection is estimated ~ 2.3 events for $20.7\,\text{fb}^{-1}$, on a total number of events in the signal region $[122, 128]$ GeV of ~ 30. The signal region is estimated as $\pm 2\sigma_{CB} = 4\,\text{GeV}$ around the peak position $m_H = 125\,\text{GeV}$.

The results for the 95% CL exclusion in fig. 3 shows that the analysis is expected to exclude a signal five times the Standard Model (dotted line). The observed exclusion (solid line) at 95% CL of σ_{obs}/σ_{SM} (σ_{obs} observed cross section and σ_{SM} Standard Model cross section with Higgs signal) is consistent with the expected value.

p_0 fluctuations are within 2σ from 1 therefore they can be classified as statistical fluctuations, there is no evidence of unforeseen signal.

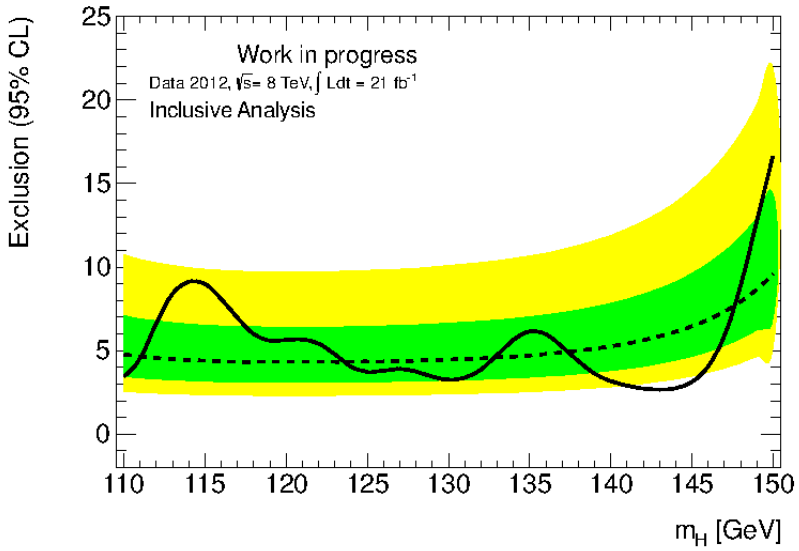

Fig. 3. – Exclusion plot of the $M_{\gamma\gamma}$ distribution of $20.7\,\mathrm{fb}^{-1}$ of statistic recorded by the ATLAS detector at CERN in the year 2012 passing diphoton + $E_T^{MISS} > 80\,\mathrm{GeV}$ selection. The dotted black line shows the 95% exclusion for SM signal (from asimov dataset) showing that the analysis is expected to exclude a signal five times the Standard Model. The darker and lighter bands indicate the corresponding 68% and 95% certainty of those values. The observed exclusion at 95% CL of σ_{obs}/σ_{SM}, solid line, is consistent with the expected value.

7. – Conclusions

I analyzed the full statistic registered in 2012 of $\mathcal{L} = 20.7\,\mathrm{fb}^{-1}$ by the ATLAS detector. In my analysis I selected a sample requiring two photons isolated and well reconstructed and an additional selection on the E_T^{MISS} of 80 GeV. My selection allows to enhance the fraction of events from associated production (W and Z) in the signal events from 5% to 50% (fig. 2). With the data available at the moment the expected number of signal events is estimated ∼2.3 for $20.7\,\mathrm{fb}^{-1}$ on a total number of events in the signal region $[122, 128]$ GeV around 30. I obtained an exclusion of 5 time the SM at 95% CL in the interval $[100, 150]$ GeV, as seen in fig. 3. The observed value of σ_{obs}/σ_{SM} is consistent with the Standard Model expectation.

REFERENCES

[1] Aad Georges *et al.* (ATLAS Collaboration), *Observation of a new particle in the search for the Standard Model Higgs boson with the ATLAS detector at the LHC*, CERN-PH-EP-2012-218.
[2] ATLAS Collaboration, *Selection for Higgs to diphoton analysis supporting note, for Moriond 2013*, ATL-COM-PHYS-2013-093.
[3] CMS Collaboration, *Observation of a new boson with mass near* 125 GeV *in pp collisions at* $s = 7$ *and* 8 TeV, CERN-PH-EP-2013-035.
[4] Sjostrand Torbjorn, Mrenna Stephen and Skands Peter Z., *A Brief Introduction to PYTHIA 8.1*, arXiv:0710.3820.

[5] Alioli Simone, Nason Paolo, Oleari Carlo and Re Emanuele, *A general framework for implementing NLO calculations in shower Monte Carlo programs: the POWHEG BOX*, arXiv:1002.2581.
[6] Toolkit for the simulation of the passage of particles through matter, `http://geant4.web.cern.ch/geant4/`.
[7] Crystal Ball Collaboration, `http://en.wikipedia.org/wiki/Crystal_Ball_function/`.
[8] ATLAS Collaboration, *Expected photon performance in the ATLAS experiment*, ATLAS-PHYS-PUB-2011-007.
[9] ATLAS Collaboration, *Performance of Missing Transverse Momentum Reconstruction in ATLAS studied in Proton-Proton Collisions recorded in 2012 at* 8 TeV, ATLAS-CONF-2013-082
[10] ATLAS Collaboration, *Observation and study of the Higgs boson candidate in the two photon decay channel with the ATLAS detector at the LHC*, ATLAS-CONF-2012-168.
[11] Cowan G., Cranmer K., Gross E. and Vitells O., *Asymptotic formulae for likelihood-based tests of new physics*, arXiv:1007.1727
[12] Wilks S. S., *The Large-Sample Distribution of the Likelihood Ratio for Testing Composite Hypotheses*, `http://www.jstor.org/stable/2957648`.
[13] Wald Abraham, *Tests of Statistical Hypotheses Concerning Several Parameters When the Number of Observations is Large*, `http://www.jstor.org/stable/1990256`.